



# Overcoming cloud obstruction: Fast forest-damage assessment in post-tropical cyclone optical remote sensing

Tianchu Wang<sup>a</sup>, Wentao Yang<sup>a,b,\*</sup>, Ziteng Xu<sup>a</sup>, Wenwen Qi<sup>c</sup>, Liam Taylor<sup>d</sup>, Ming Wang<sup>e,f</sup>, Wei Wu<sup>g</sup>

<sup>a</sup> Three-gorges reservoir area (Jinyun Mountain, Chongqing) Forest Ecosystem National Observation and Research Station, School of Soil and Water Conservation, Beijing Forestry University, Beijing 100083, China

<sup>b</sup> Academy of Plateau Science and Sustainability, People's Government of Qinghai Province and Beijing Normal University, Xining 810016, China

<sup>c</sup> National Institute of Natural Hazards, Ministry of Emergency Management of China, Beijing 100085, China

<sup>d</sup> School of Geography, University of Leeds, Leeds LS2 9JT, UK

<sup>e</sup> School of National Safety and Emergency Management, Beijing Normal University, Beijing 100875, China

<sup>f</sup> Joint International Research Laboratory of Catastrophe Simulation and Systemic Risk Governance, Beijing Normal University at Zhuhai, Zhuhai 519087, China

<sup>g</sup> National Disaster Reduction Center, Ministry of Emergency Management of China, Beijing 100124, China

## ARTICLE INFO

### Keywords:

Post-hazard assessment  
Fast mapping  
Machine learning  
Remote sensing

## ABSTRACT

Timely mapping of damaged forests is critical for disaster assessment. However, remote sensing data immediately after natural hazards is always scarce and susceptible to cloud contamination, hindering holistic assessment of damaged forests in a timely manner. Herein, we propose a novel method to map damaged forests obscured by clouds in post-hazard images by taking the September 2024 typhoon Yagi in Hainan Island, China as an example. Our approach uniquely integrates observed forest damage in cloud-free pixels with its influencing factors (the maximum wind speed and cumulative rainfall during the typhoon, terrain (elevation, slope and aspect), and canopy height) to interpolate the relationship into cloud-covered pixels by using three mainstream machine learning models (XGBoost, artificial neural networks and random forest). We found severe forest damage in the Northeast Hainan and the total area of the typhoon-damaged forests accounts for 12.8%–15.5% of the island's forest cover. This method can also be used for fast mapping of forest damage in partially available remote sensing images after other major natural hazards such as wildfires and landslides

## 1. Introduction

Annually, tropical cyclones inflict substantial economic losses on world's coastal regions (Achu et al., 2021; Ansari et al., 2025; Howe et al., 2025; Liu et al., 2024; Salim et al., 2024; Xu et al., 2015; Sonet et al., 2024). Their wide footprint (100 s km across), high magnitude (wind speeds ranging from 119 to 250+ km/h), and long tracks (1000s km) mean that tropical cyclones can cause widespread destruction to natural ecosystems such as coastal forests (Feng et al., 2020). Given the likely increase in frequency and intensity of tropical cyclones as the climate changes (Bhatia et al., 2022; Sobel et al., 2016), this impact on the natural environment is also likely to increase (Mendelsohn et al., 2012). In the immediate aftermath of a tropical cyclone, rapid and objective assessments of damaged forests hold critical significance for

decision-makers to formulate evidence-based strategies for disaster mitigation.

Bottom-up approaches are frequently used to estimate post-hazard damage following major disasters, where estimated damage by the local communities is passed to the upper administrative departments, which sum up and offer a holistic total assessment for decision-makers. However, this process is time-consuming, labour-intensive, and subjective (Khajwal and Noshadravan, 2021). Timely mapping of damaged forests in an objective and holistic way is critical for disaster assessment and to support on-the-ground recovery programmes.

Remote sensing technologies could provide objective and reliable means for large-scale forest damage assessments (Hayashi et al., 2015; Upadhyay and Kumar, 2018). While radar data can help establish timelines for tree damage (Burrows et al., 2023), its utility is constrained

\* Corresponding author at: Three-gorges reservoir area (Jinyun Mountain, Chongqing) Forest Ecosystem National Observation and Research Station, School of Soil and Water Conservation, Beijing Forestry University, Beijing 100083, China.

E-mail address: [yang\\_wentao@bjfu.edu.cn](mailto:yang_wentao@bjfu.edu.cn) (W. Yang).

<https://doi.org/10.1016/j.ecoinf.2025.103252>

Received 25 March 2025; Received in revised form 30 May 2025; Accepted 30 May 2025

Available online 2 June 2025

1574-9541/© 2025 The Authors. Published by Elsevier B.V. This is an open access article under the CC BY-NC license (<http://creativecommons.org/licenses/by-nc/4.0/>).

by inherent speckle noise and limitations in identifying precise locations of damaged forests. The application of SAR remains in an exploratory stage in forest damage monitoring and, due to the complexity of data interpretation, the reliability of monitoring results is still under debate (Tanase et al., 2018; Tomppo et al., 2021). Optical remote sensing imagery has proven effective in evaluating forest damage from natural hazards such as landslides (Qi et al., 2020; Yang et al., 2013), tropical cyclones (Lu et al., 2020; Wang and Xu, 2018), fires and climatic changes (Bochenek et al., 2015a).

Vegetation indices (such as the Normalized Difference Vegetation Index; NDVI) are derived from pre- and post-hazard optical images and are used to efficiently map vegetation damage (Bartold, 2012; Chen et al., 2022; Lee et al., 2008; Yang et al., 2013; Zhang et al., 2022). Bartold (2012) utilized Terra MODIS satellite remote sensing data to monitor forest damage in Poland and Slovakia, demonstrating that NDVI data from a low spatial resolution optical image (250 m) can achieve high monitoring accuracy. With the advancement of satellite remote sensing technology, the monitoring of terrestrial vegetation using NDVI has gradually evolved from the utilization of low-resolution data sources such as NOAA (Bochenek et al., 2015b) and MODIS (Schnur et al., 2010; Sun et al., 2011) to higher-resolution data sources such as Landsat (Anees et al., 2024; Dimson et al., 2024) and SPOT (Li et al., 2024). Currently, Sentinel-2 data represents one of the highest resolutions publicly available optical remote sensing datasets (10 m resolution) and is adept at monitoring vegetation change following disaster (Eskandari and Sarab, 2022; Leisenheimer et al., 2024; Zhang et al., 2024).

Most previous works use cloud-free optical images to detect vegetation stress (e.g., Bartold and Kluczek, 2024). However, optical images are vulnerable to adverse weather conditions such as cloud cover, hindering complete spatial coverage of hazard-affected areas (Li et al., 2020; Meraner et al., 2020). This limitation is particularly acute following tropical cyclone events, where affected areas typically experience extensive and prolonged cloud obstruction for days following initial impact. Although algorithms exist to recover cloud-covered information in target remote sensing images, these methods primarily rely on archived images of other periods that have not experienced land cover change (Hu and Smith, 2018; Kang et al., 2016; Li et al., 2019). Such approaches require multiple clear post-hazard images, making it challenging to rapidly map post-hazard forest damage holistically.

Machine learning models that use geospatial variables to model hazard susceptibilities/risks (Sarkar et al., 2024) paved the way to map cloud-covered forest damage in post-hazard images. Random Forest (RF) is widely applied in the areas of forest fire prediction (Bhadoria et al., 2021; Zahura et al., 2024), and Artificial Neural Networks (ANN) have been utilized in modelling for forest disaster prediction (Achu et al., 2021).

On 5 September 2024, Super Typhoon Yagi made landfall on Hainan Island, China causing extensive damage to local forests. Official reports confirmed 4 fatalities, 95 injuries, and direct economic losses exceeding ¥59.024 billion in Hainan by 7 September (China Meteorological News Press, 2024-9-8). At the time of impact, Typhoon Yagi was the second-most powerful typhoon to strike the island, surpassed only by the Super Typhoon Rammasun in 2014. Coastal shelterbelts along the eastern Hainan suffered near-complete destruction, with varying degrees of forest damage across the province. Following the hazard, authorities promptly generated a rough damage estimation through the abovementioned bottom-up approach. However, this estimation is known to contain substantial errors, including discrepancies in statistical criteria across different administrative regions and reliance on subjective judgements in large areas due to operational constraints at the community level. Therefore, there is great urgency to rapidly and accurately quantify this super typhoon's impacts on forest cover. By using Typhoon Yagi as an example, this study aims to develop a method to map typhoon-damaged forests in a timely and objective manner by overcoming cloud obstacles in post-hazard remote sensing images.

## 2. The study area and the typhoon Yagi

Hainan Island is the largest island in the South China Sea with an area of approximately 33,210 km<sup>2</sup>. The island's topography features a central highland (peaking at 1867 m in Wuzhi Mountain) surrounded by lower elevations (Hainan Historical and Cultural Website, 2024-2-28). It has a maritime tropical monsoon climate (Guo et al., 2021) with an annual average temperature of 24.8 °C and mean precipitation exceeding 1800 mm. Precipitation patterns exhibit strong spatial variability: influenced by summer monsoons and orographic effects, rainfall decreases from east to west, with the eastern regions receiving the highest accumulations and the southwest being comparatively drier (Xu et al., 2013).

According to a land-use data from 2023 (Yang and Huang, 2021), Hainan's total forested area is 22,113 km<sup>2</sup>, accounting for 67 % of the island's total land area. The zonal vegetation consists of tropical monsoon forests, though diverse microclimates driven by topographic complexity support varied ecosystems. Coastal shelterbelts encircle the island, while extensive plantations of commercial tree species dominate inland areas (Yang et al., 2021). According to a report by the Hainan Provincial Forestry Bureau (2023), the province's forestry sector generated ¥53.583 billion in annual output.

Super Typhoon Yagi (International designation: 2411; Joint Typhoon Warning Center: WP122024) was the 11th named storm of the 2024 Pacific typhoon season. According to the China Meteorological Administration (China Meteorological Administration, 2024-9-6), a tropical disturbance formed over the western Pacific, east of Mindanao Island, Philippines, on 30 August 2024. It intensified into a tropical depression by 1 September, further strengthening to tropical storm status on 2 September. At 14:00 local time that day, Typhoon Yagi made its first landfall in Casiguran, Aurora Province, Philippines, temporarily weakening before entering the South China Sea.

By 3 September, Yagi re-intensified to a severe tropical storm over the South China Sea. By 23:00 of 4 September, it intensified to become a super typhoon. At 16:20 local time on 6 September, the super typhoon struck Wenchang City, Hainan Province, China, with maximum sustained winds of 62 m/s at landfall. It made a second landfall later in Xuwen County, Guangdong Province, before weakening slightly and striking southern Quảng Ninh Province, Vietnam, on 7 September with winds of 58 m/s (see Fig. 1 for storm trajectory).

## 3. Methodology

### 3.1. Data

This study utilized Sentinel-2 imagery, topographic data, and meteorological data (Table 1) to assess the impact of Super Typhoon Yagi on Hainan. The high-resolution Multispectral Imager (MSI) aboard Sentinel-2 offers observational capabilities across 13 bands ranging from visible to infrared light, with a revisit period of five days. Among these, the visible and near-infrared bands have a spatial resolution of 10 m, which are used to monitor vegetation through an NDVI. We obtained Sentinel-2 Band 4 (red) and Band 8 (near-infrared) data from Google Earth Engine (GEE), which provides Level-2 A products that have undergone atmospheric correction with the ESA's official, state-of-the-art Sen2Cor (Louis et al., 2021; Main-Knorn et al., 2017).

We identified 13 pre-typhoon images with the lowest cloud coverage (~0 % in cloud cover percentage) from 2016 to 2024 across different seasons to ensure an accurate representation of seasonal fluctuations in vegetation (Table 2). Cloud-free post-typhoon Sentinel-2 images were more limited, with the best available image taken 20 days later (13 September 2024), but still partially covered by clouds. To ensure that our model remained accurate, despite only using one post-typhoon image, we set strict cloud probability threshold of <5 to reserve the highest quality pixels in the post-hazard image (Fig. 2i). With this threshold, approximately 78 % of the post-typhoon image is covered by

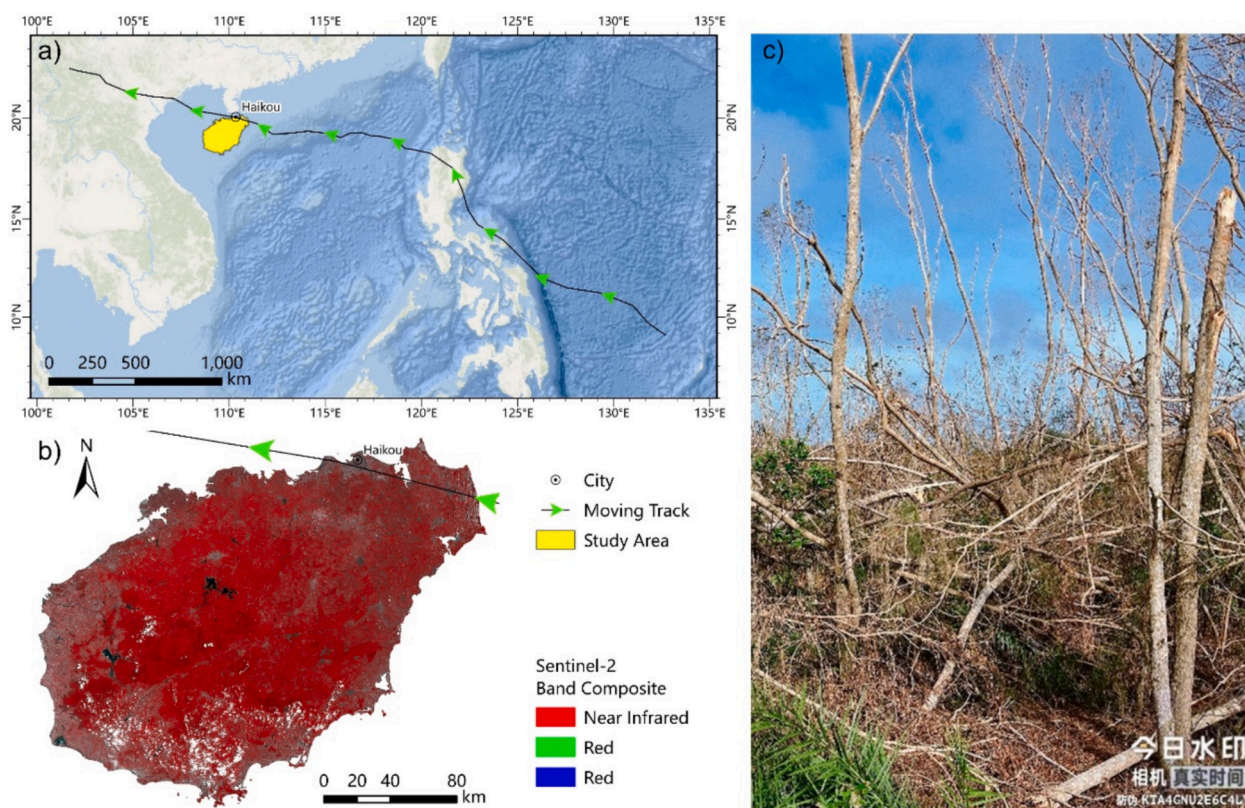


Fig. 1. Moving track of the Super Typhoon Yagi (a) and a false colour composite of the affected Hainan Island (b). Photo of typhoon-damaged forest (c). The photo was taken by the author on 20 September 2024 in the East Island’s Forest Farm.

**Table 1**  
Geospatial data used in this study.

Data	Resolution (m)	Source
DEM	30	NASA / USGS / JPL-Caltech ( <a href="https://lpdaac.usgs.gov/products/nasadem_hgtv001/">https://lpdaac.usgs.gov/products/nasadem_hgtv001/</a> )
Slope	30	Calculated by DEM
Aspect	30	Calculated by DEM
NDVI	10	Calculated from Sentinel-2 images (Table 2)
Canopy height	10	ETH Global Sentinel-2 10 m Canopy Height (2020)
Wind velocity	10	China Meteorological Administration
Precipitation	10	China Meteorological Administration
Forest boundary	/	Hainan Forestry Bureau

**Table 2**  
Dates of all Sentinel-2 images used in this study. There is only one post-hazard image, which is underlined.

2/6/2016	5/10/2018	13/3/2020	23/3/2023	1/4/2024
19/12/2017	30/10/2018	22/5/2021	22/5/2023	<u>13/9/2024</u>
13/4/2018	30/9/2019	20/8/2021	21/2/2024	

clouds and will be recovered by our algorithm. While further images would be available in time, the need for a rapid assessment to support on-the-ground efforts accentuates the need to build a model that can handle sub-optimal imagery. All data underwent foundational pre-processing on GEE, including spatial clipping and mosaicking, followed by NDVI analysis.

Digital Elevation Model (DEM) data for Hainan Island at 30 m spatial resolution were sourced from the NASA/USGS/JPL-Caltech dataset on

GEE. Slope and aspect derivatives were subsequently calculated within GEE at the same 30 m resolution. Canopy height data were sourced from the ETH Global Sentinel-2 10 m Canopy Height dataset (Lang et al., 2023), which provides global canopy height data for the year 2020 at a spatial resolution of 10 m. Meteorological data - including typhoon-induced wind speeds and cumulative precipitation - were acquired from the China Meteorological Administration. Forest stand boundaries were provided as vector data by the Hainan Forestry Bureau. For model training, 29,865 sample points were randomly generated within the cloud-free portion of our post-typhoon Sentinel-2 image. All datasets are spatially illustrated in Fig. 2.

### 3.2. Methods

The methodological workflow comprises three key steps (Fig. 3). In the first step, we calculated NDVI for all selected pre-hazard images and established Harmonic Regression Models (HRM) by using these pre-typhoon NDVI for each pixel in the study area. Root Mean Square Errors (RMSE) of harmonic models were assessed by the difference between the modelled and observed pre-hazard NDVI. In the second step, because the first available post-hazard image was acquired on 13 September 2024, we simulated undisturbed NDVI values on that day with harmonic models of each pixel. For cloud-free pixels on the pre-hazard image, we calculated  $\Delta$ NDVI by subtracting the derived NDVI from the harmonic model simulated NDVI to define the Forest Damage Index (FDI). In the last step, we train three machine learning models by using FDI from the last step and its influencing factors. We then leverage these machine learning models to map FDI obscured by clouds in the post-hazard image.

#### 3.2.1. Pre-hazard NDVI modelling

The NDVI was adopted to characterize the status of surface vegetation. Numerous studies have demonstrated the robustness of NDVI in

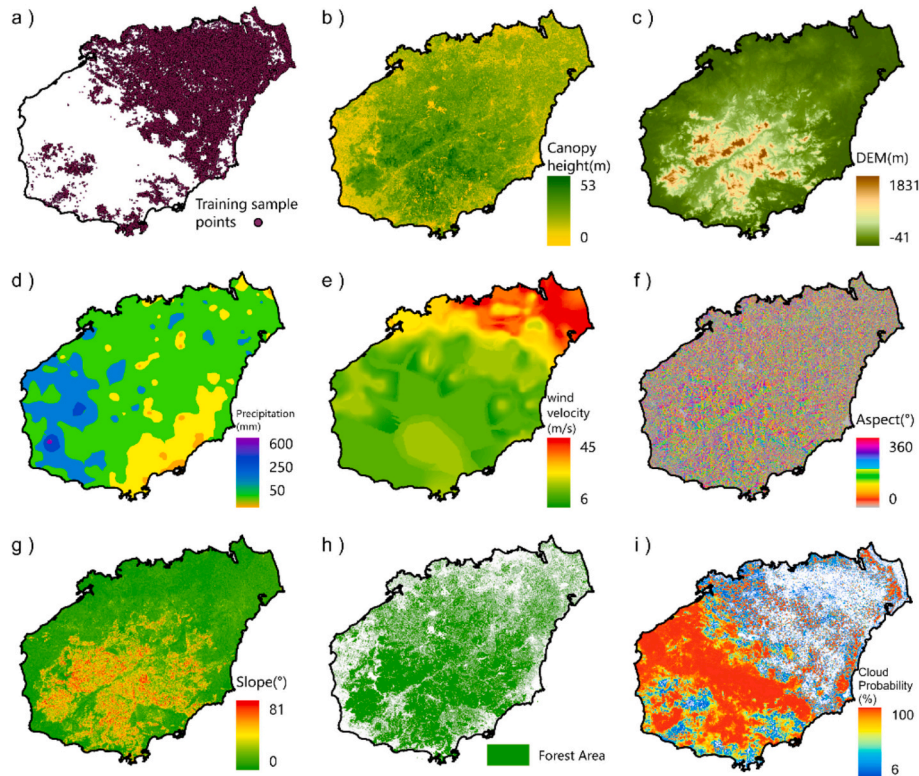


**Fig. 2.** Factors that could influence forest damage assessment. Sampling points to build the machine learning models were located in cloud-free locations of the Sentinel-2 image acquired on 13 September 2024 (a). Canopy height ranges from 0 to 53 m on the island (b). The DEM(c), aspect (f) and slope (g) maps. This typhoon led to ~600 mm cumulative precipitation in the southwest part of the island (d). High winds (>30 m/s) were recorded during this typhoon (e). Forests is a major land cover type in the island (h). In the optical remote sensing imagery captured by Sentinel-2 on 13 September 2024, the area with a cloud probability exceeding 5 constituted approximately 78 % of the total area of Hainan Island (i).

reflecting vegetation health while being minimally affected by illumination variations (Hou et al., 2022; Konatowska et al., 2023; Mehmood et al., 2024). According to field survey results (Fig. 1c), the forests in the eastern part of Hainan were nearly destroyed. Such severe disturbances make the NDVI adequate to meet our monitoring needs without the need to consider the issue of NDVI saturation (Liu and Huete, 1995). The NDVI is calculated as follows:

$$NDVI = \frac{NIR - RED}{NIR + RED} \quad (1)$$

where NIR (Near-Infrared) and RED correspond to the surface reflectance values of Sentinel-2's Band 8 (~842 nm) and Band 4 (~665 nm), respectively. The NDVI ranges from -1 to 1: higher values indicate healthier vegetation, lower values suggest stressed or sparse vegetation, and negative values typically represent water bodies or snow/ice cover.

To simulate pre-hazard vegetation conditions on any date, we build HRM with all 13 pre-disaster Sentinel-2 images. The HRM is one of the frequently used time-series models that could mimic NDVI changes by considering seasonal changes and trends (Qi and Xu, 2020). It (HRM) was first proposed by Zhu and Woodcock (2014) for outlier detections in time series of Landsat images and was later modified by Qi and Xu (2020) to fit seasonal changes in NDVI time series. The HRM is formulated as:

$$NDVI(t) = \beta_0 + \beta_1 t + \beta_2 \cos(2\pi t) + \beta_3 \sin(2\pi t) \quad (2)$$

where  $\beta_0$  represents the constant term, indicating the baseline NDVI value.  $\beta_1$  denotes the linear trend coefficient, representing the linear change of NDVI over time.  $\beta_2$  and  $\beta_3$  are harmonic coefficients, indicating the periodic fluctuations of NDVI.  $t$  represents time.

This study uses RMSEs to evaluate the performance of the HRMs. The

calculation formula is as follows:

$$RMSE = \sqrt{\frac{1}{n} \sum_{t=1}^n (y_i - \hat{y}_i)^2} \quad (3)$$

where  $y_i$  represents the true NDVI value, and  $\hat{y}_i$  is the predicted value by the HRM.

### 3.2.2. Forest damage index (FDI) calculation

HRMs could simulate NDVIs not disturbed by the typhoon. The difference between the true NDVI derived from a post-hazard image and the simulated, "undisturbed" value of the same date represents the typhoon caused damage. We predicted the NDVI data on 13 September 2024 with the HRMs, and then calculated the difference between observed and predicted NDVI. This NDVI difference ( $\Delta NDVI$  used interchangeably with the FDI throughout this work), was used to characterize the impact of the Super Typhoon Yagi on the vegetation of Hainan Island. The formula for calculating FDI is as follows:

$$FDI = \Delta NDVI = NDVI_{predict} - NDVI_{true} \quad (4)$$

where  $NDVI_{predict}$  represents the NDVI data predicted by the HRM, and  $NDVI_{true}$  represents the actual observed NDVI data for the day.

In this study, we used 13 NDVI images from before the disaster to fit the HRM and predict the NDVI for 13 September 2024 as  $NDVI_{predict}$ . The cloud-free NDVI data observed from Sentinel-2 optical remote sensing imagery on 13 September 2024 was used as  $NDVI_{true}$  to calculate FDI.

### 3.2.3. Machine learning models to map FDI under clouds

After applying the cloud probability mask, ~78 % of the post-hazard Sentinel-2 image was removed, rendering spatially incomplete FDI. To fill this data gap, we constructed 29,865 random sample points in the

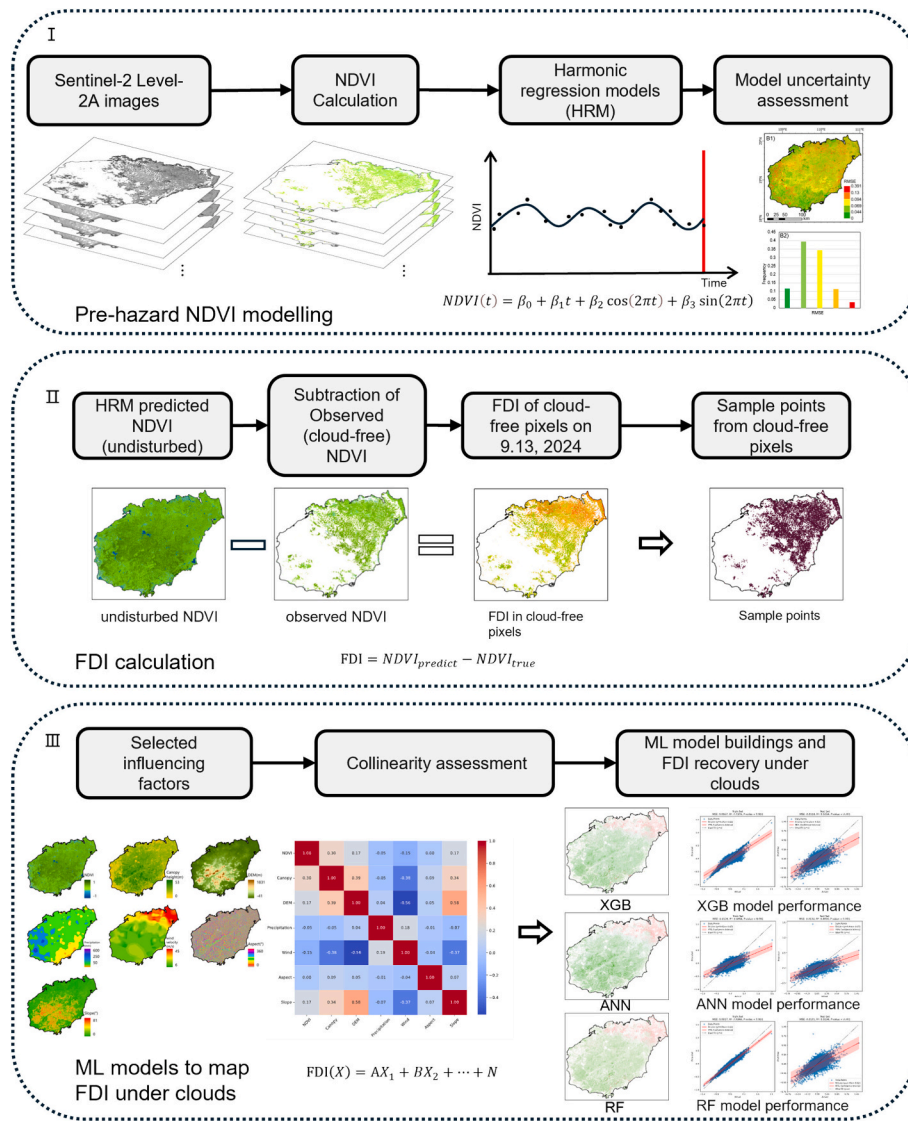


Fig. 3. Flowchart of the work.

cloud-free pixel with FDI values. Additionally, we utilized factors such as NDVI (predicted by the HRM), canopy height, elevation, precipitation, wind velocity, aspect, and slope as independent variables to create the training set. We employed this training set to train the XGB, ANN, and RF regression models (Breiman, 2001; Chen and Guestrin, 2016; Setiono et al., 2002), and then applied them to predict spatially missing FDIs across the study area, achieving full-coverage assessment of forest damage caused by the typhoon.

During the model training process, the Mean Squared Error (MSE), the coefficient of determination ( $R^2$ ), and the significance test  $p$ -value are utilized as indices to evaluate the effectiveness of the model training. The model training error is quantitatively expressed using the MSE, which is defined as follows:

$$MSE = \frac{1}{n} \sum_{i=1}^n (y_i - \hat{y}_i)^2 \quad (5)$$

where  $y_i$  represents the true value, and  $\hat{y}_i$  is the predicted value by the model. In this study, 70 % of the data was designated as the training set, while the remaining 30 % was used as the test set.

The hyperparameter settings of machine learning models directly influence their training effectiveness. In this study, after multiple trials, we selected what we deemed to be the most appropriate

hyperparameters. For training RF model, we constructed 100 random trees. The ANN model that we employed consists of an input layer, two hidden layers (with the first hidden layer comprising 64 neurons and the second hidden layer comprising 32 neurons, both utilizing the ReLU activation function), and an output layer containing one neuron designed to output continuous values. Training was halted when the errors no longer decreased to avoid overfitting. For training XGB model, the maximum depth of each tree was set to 6, and the learning rate was set to 0.1. During our process, forest stand boundaries provided by the Hainan Forestry Bureau were used to ensure all assessments were made for forests.

## 4. Results

### 4.1. Performance of different machine learning models

Using the HRM, this study successfully derived the undisturbed NDVI for the Hainan Island on 13 September 2024 (Fig. 4A). The RMSEs of the vast majority of regions were distributed within the range of 0 to 0.1, indicating that the HRM had a good predictive effect (Fig. 4 B1&B2). The typhoon-induced NDVI change ( $\Delta NDVI$ ) was calculated by subtracting the observed NDVI on 13 September 2024 from the HRM-predicted baseline, though there existed extensive data gaps due to

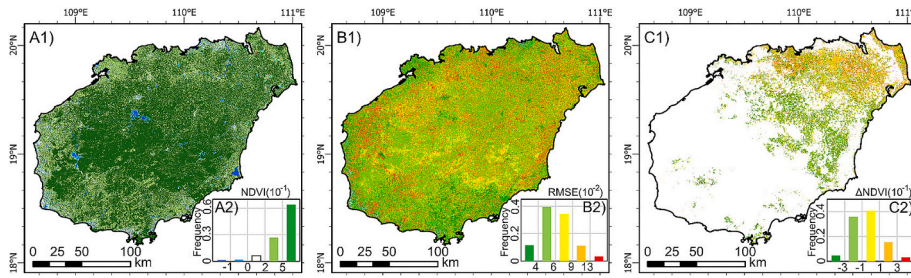


**Fig. 4.** Modelled NDVI on 13 September 2024 by harmonic regression models (HRM) (A) and calculated  $\Delta$ NDVI (Forest Damage Index, FDI) with the post-typhoon Sentinel-2 image of the same date for pixels free of clouds (C). The distribution of RMSE in the HRM calculated by pixel (B1). Most of the RMSEs of HRMs fitting NDVI are in the range of 0 to 0.1 (B2).

persistent cloud cover (Fig. 4C). Notably, large areas of  $\Delta$ NDVI data are missing, particularly in the central and southwest parts of the island.

We employed XGB, ANN, and RF models to predict missing  $\Delta$ NDVI values in cloud-affected areas.  $\Delta$ NDVI was utilized as the FDI for assessing forest damage. The selected influencing factors (independent variables) in this study - NDVI, canopy height, DEM, precipitation, wind velocity, aspect, and slope - exhibited low pairwise correlations, as demonstrated in Fig. 5. In addition to the high positive correlation (0.58) between DEM and slope, as well as the high negative correlation ( $-0.56$ ) between DEM and wind velocity, the correlations among other factors are generally low. This minimal multicollinearity ensures that the predictive performance of the machine learning models (XGB, ANN, RF) are not compromised by redundant explanatory factors, thereby enhancing the reliability of the derived  $\Delta$ NDVI predictions.

In this study, XGB, ANN, and RF regression models were trained on the same training set. The MSE was used to evaluate the performances of the model training results, as shown in Fig. 6. We found that the MSE of the XGB model on the training set was 0.0067 and on the test set was 0.0118, indicating a good model prediction performance. The MSE of the ANN model on the training set was 0.0128 and on the test set was 0.0134, which was the worst among the three models. The MSE of the RF model on the training set was 0.0017 and on the test set was 0.0121, indicating a good model prediction performance. In terms of the coefficient of determination ( $R^2$ ), we found that the RF model achieved an  $R^2$  of 0.9346 on the training set and 0.5196 on the test set. The XGB model demonstrated an  $R^2$  of 0.7376 on the training set and 0.5334 on the test

set. The ANN model achieved an  $R^2$  of 0.4964 on the training set and 0.4696 on the test set. Considering the MSE and  $R^2$  performance of the training and test sets of the three models comprehensively, we believe that in this study, the RF model demonstrates superior predictive performance while maintaining high training accuracy. Conversely, although the XGB model exhibits lower training performance compared to the RF model on the same training dataset, it achieves predictive performance that is comparable to or even surpasses that of the RF model despite its lower training accuracy. In summary, both the RF and XGB models effectively simulate the changes in the NDVI following Super Typhoon Yagi. In contrast, the ANN model exhibits weaker predictive performance than both the RF and XGB models. The significance tests for all three models indicate that their results are highly significant ( $p \leq 0.001$ ).

Due to the poor interpretability of the ANN model, the factor contributions cannot be directly calculated. Only RF and XGB can produce factor contributions (Fig. 7). In both the RF and XGB models, NDVI and wind velocity have the highest contributions, contributing  $>70\%$  in combination. Wind velocity, as a triggering factor for forest damage, having a high contribution is reasonable. Higher NDVI contribution means that the vegetation condition is very susceptible to natural hazards. Among the three factors that characterize terrain features, slope has the highest contribution.

#### 4.2. Distribution of typhoon-damaged forests

Fig. 8 shows the spatial distribution of the FDI from the XGB, ANN, and RF models. Most of the northeast of Hainan Island has a positive FDI, indicating extensive forest damage. In contrast, most of the central and southwest parts of the island were unaffected ( $FDI < 0$ ). Percentages of area with positive FDI from these three models are spatially consistent with each other ranging from 12.8% to 15.5%. ANN mapped the least area of damaged forests and RF mapped the largest area.

To demonstrate the capability of these models in supporting on-the-ground disaster recovery efforts, we selected two of the most severely affected areas, Wenchang City and the East Island's Forest Farm, in the northeast of the island to demonstrate finer details of forest damage. Both of these areas experienced significant forest damage as they were among the first to be hit by Super Typhoon Yagi. We conducted a comparative analysis of the differences in the area distribution of the FDI in Wenchang City and the East Island's Forest Farm from XGB, ANN, and RF models.

As shown in Fig. 9, the XGB model indicates that  $\sim 52.73 \text{ km}^2$  of the coastal part of the East Island's Forest Farm has positive FDI (forest damage), accounting for 79.5% of the coastal area of the forest farm. Across Wenchang City,  $\sim 812.83 \text{ km}^2$  of forest area showed positive FDI, representing 75% of the total forest area. Fig. 9II illustrates that, according to the ANN model's results, the coastal part of the East Island's Forest Farm with positive FDI is  $\sim 50.95 \text{ km}^2$ , covering 79.6% of the coastal area. The entire Wenchang City has  $\sim 832.323 \text{ km}^2$  positive FDI, which constitutes 77.5% of the city's total area. Fig. 9 (III) shows that

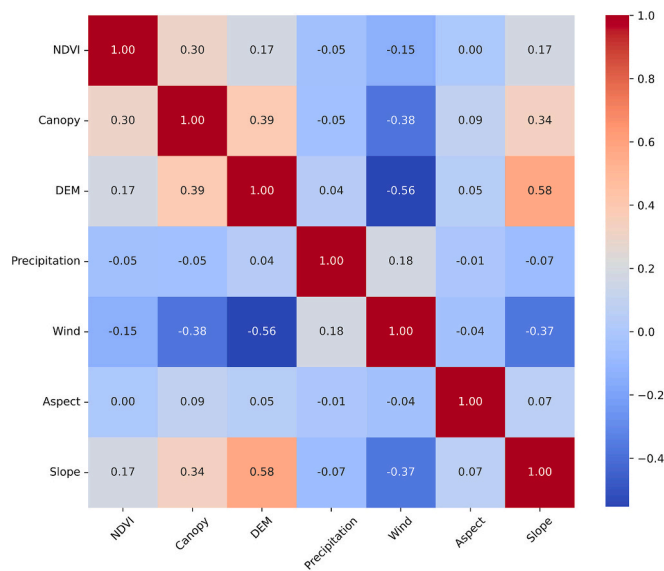


**Fig. 5.** Correlations among influencing factors that were used to model typhoon-damaged forests. The highest absolute correlations were found between DEM and slope (0.58) and between DEM and wind velocity ( $-0.56$ ).

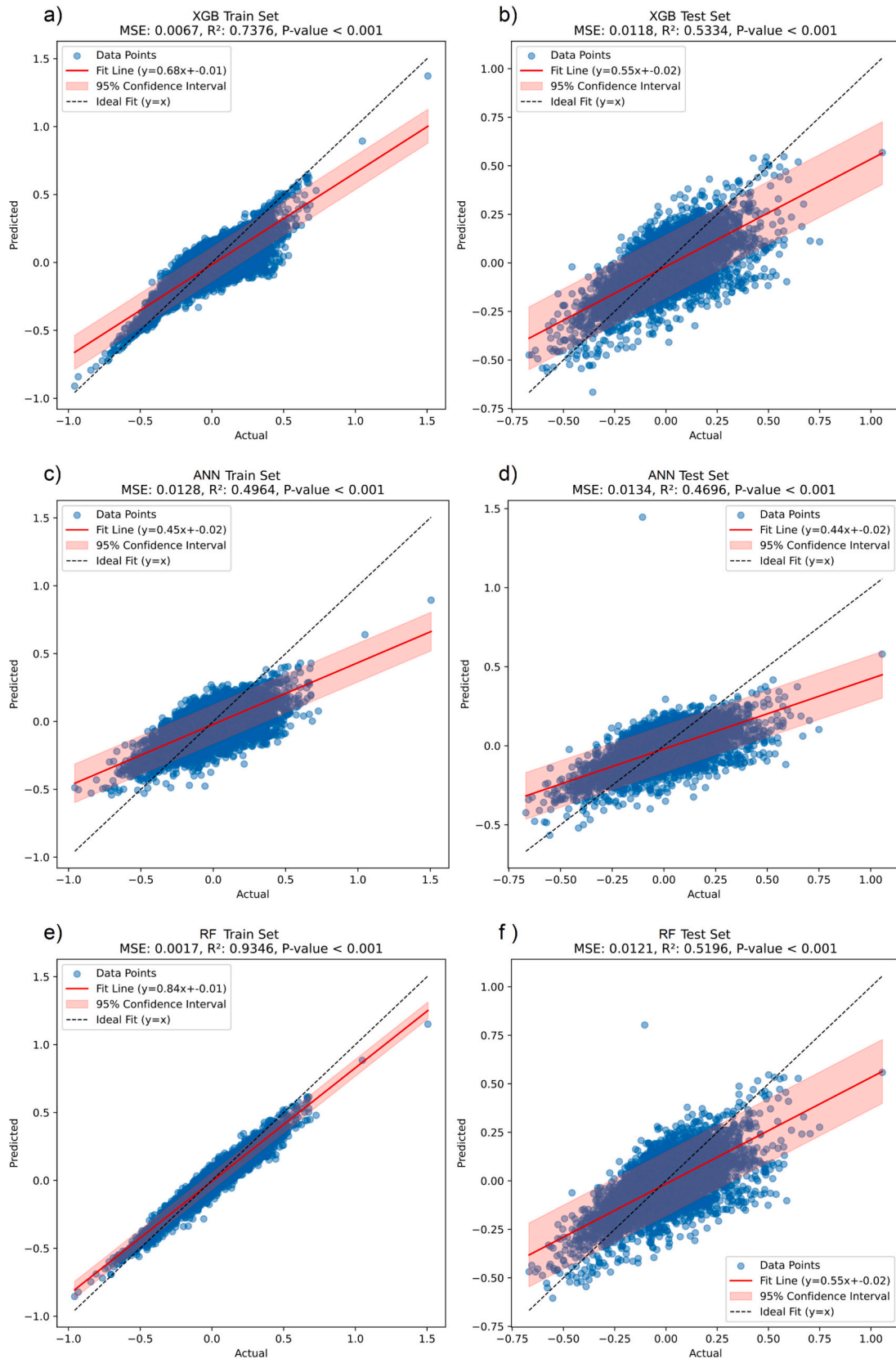


**Fig. 6.** Model performances on Training and Testing sets. a) and b) are the performances of the training and test sets of the XGBoost (XGB) model. c) and d) are the performances of the training and test sets of the Artificial Neural Networks (ANN) model. e) and f) are the performances of the training and test sets of the Random Forest (RF) model.

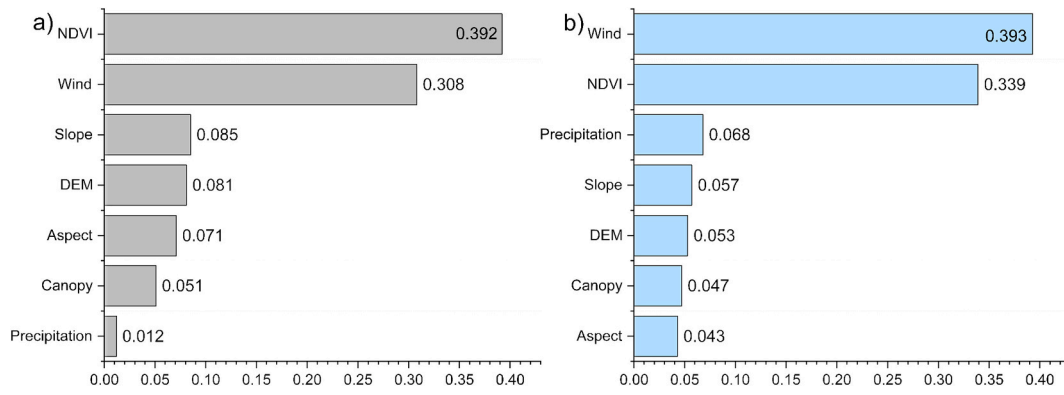


Fig. 7. Factor contributions in RF (a) and XGB (b) models. NDVI and wind velocity are the most important factors in assessing forest damage caused by the typhoon.

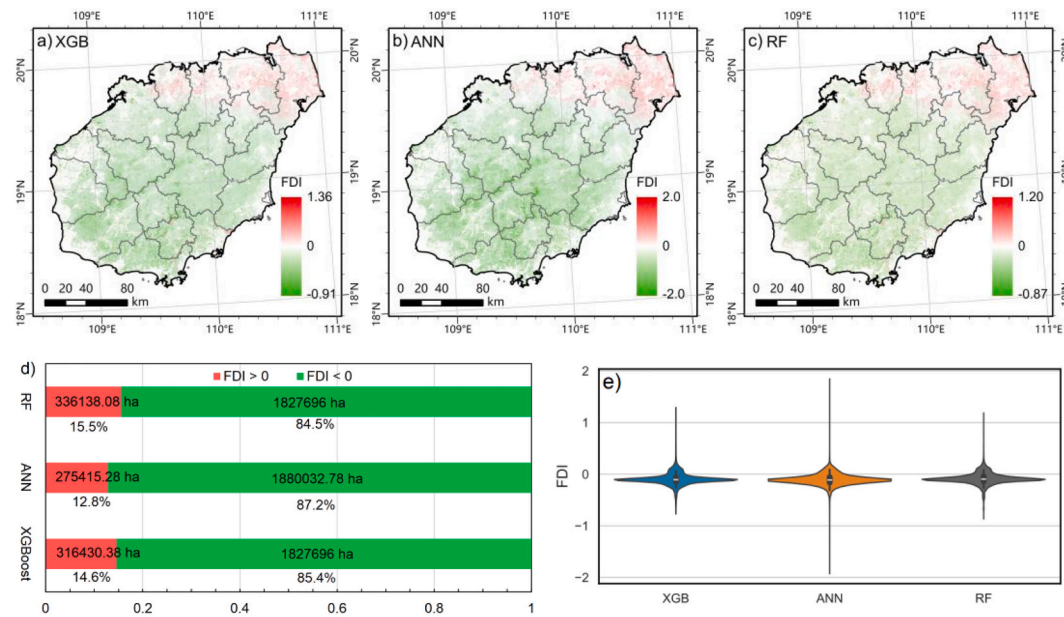


Fig. 8. FDI prediction results of XGB (a), ANN (b) and RF (c) for the Hainan Island. (d) The area proportion of the predicted FDI of the three models. (e) Data distribution of the three models for predicting the FDI.

the RF model results reveal ~51.10 km<sup>2</sup> of the coastal part of the East Island’s Forest Farm with positive FDI, accounting for 77 % of the coastal area. In Wenchang City, ~815.39 km<sup>2</sup> has a positive FDI, making up 75.3 % of the city’s area.

By comparing the results of three models - XGB, ANN, and RF - in Wenchang City, our study finds that the predictions of these models exhibit spatial consistency. The calculations damaged forest area are similar across the three models, with positive FDI area in Wenchang City ranging from ~812.83 km<sup>2</sup> to ~832.33 km<sup>2</sup>. For East Island’s Forest Farm, the positive FDI area is between ~50.96 km<sup>2</sup> and ~ 52.74 km<sup>2</sup>. Excluding the ANN model, which had poorer predictive performance, the damaged forest area in Wenchang City ranges from ~812.84 km<sup>2</sup> to ~815.39 km<sup>2</sup>, accounting for 75.0 % to 75.3 % of the city’s total forest area. In East Island’s Forest Farm, the damaged forest area ranges from ~51.11 km<sup>2</sup> to 52.74 km<sup>2</sup>, representing 77 % to 79.5 % of the forest farm’s area. (See Table 3)

We constructed line graphs of FDI distribution for East Island’s Forest Farm and Wenchang City, as illustrated in Fig. 10. For East Island’s Forest Farm, it was observed that the results from XGB and RF models exhibit similar distribution characteristics, with FDI concentrated within the 0–0.2 range and a notable increase between 0.4 and 0.6. In contrast, the ANN model’s FDI results are concentrated within the 0–0.3 range,

with a smoother distribution curve and no abrupt changes. Based on the analysis of model training performance, the study concludes that the XGB and RF models more accurately reflect the actual forest damage situation. The ANN model’s predictive performance in this study is inferior to the other two models. For the forest land in Wenchang City, the results from all three models are concentrated in the 0–0.2 range. The ANN model produces smoother calculation results, whereas the XGB and RF models retain more detailed distribution characteristics.

## 5. Discussion

### 5.1. Rapid mapping of tropical cyclone damaged forests covered by clouds

Remote sensing is a critical technique in mapping large-scale forest damage caused by tropical cyclones. However, post-hazard adverse weather conditions often hinder the timely and comprehensive assessment of hazard impacts. Machine learning models have been widely used to map forest damage areas from cloud-free optical remote sensing images (Chen et al., 2022; Zhang et al., 2021). While these studies have achieved relatively accurate estimations of forest damage areas (Bartold and Kluczek, 2024), they can only rely on cloud-free optical images and cannot provide rapid and accurate assessments of forest damage when

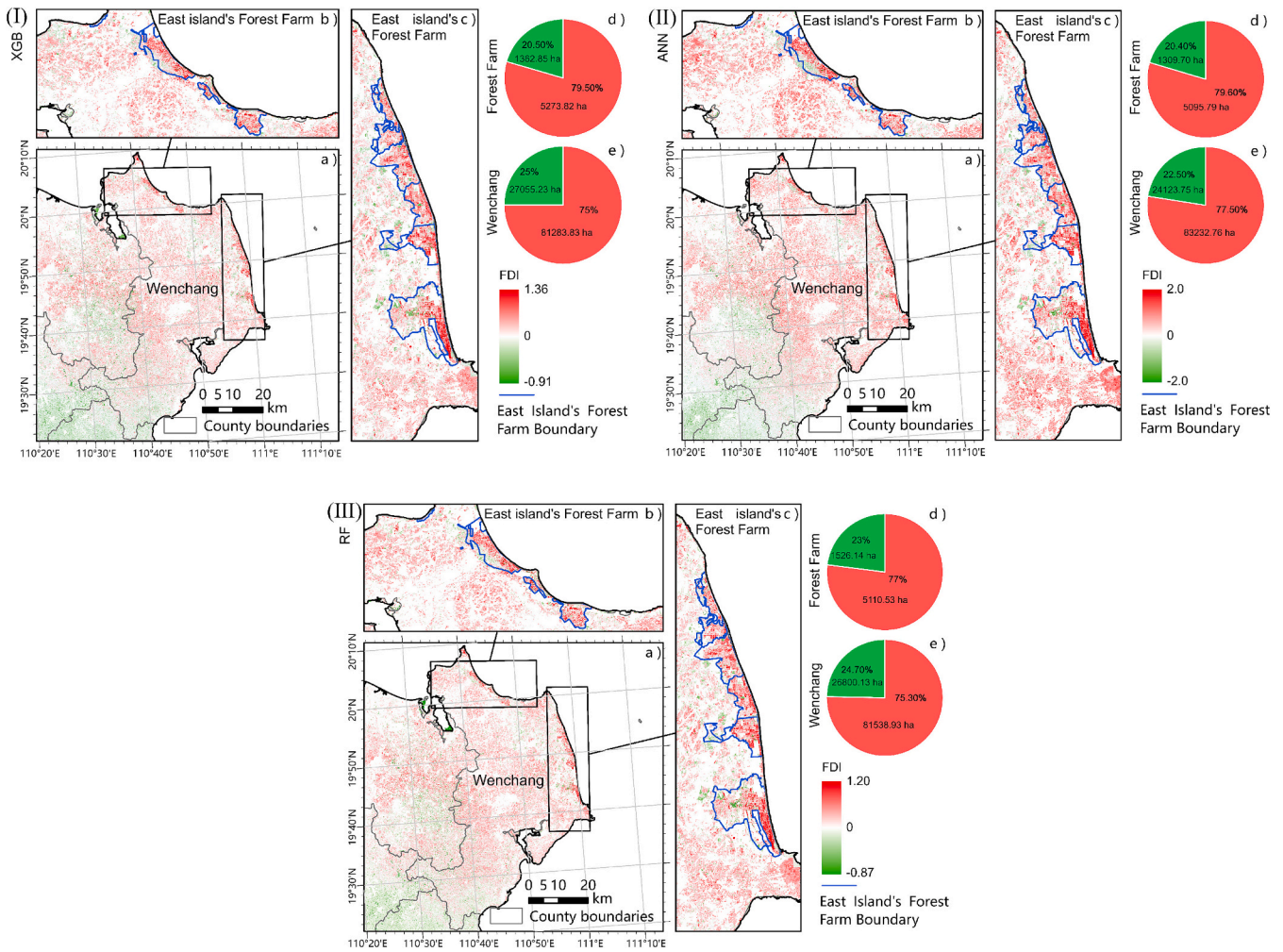


**Fig. 9.** Highlighted forest-damaged regions in north Hainan Island. Panel (I-III) show results from the XGB, ANN and RF models, respectively. In each panel, FDI in Wenchang City (a), the northern part (b) and the eastern part of the East Island's Forest Farm were shown. The proportion of different damage degrees for the East Island's Forest Farm and the Wenchang City were shown in (d) and (e), respectively.

**Table 3**

The proportion of area with FDI > 0 in different regions and different model results.

	Hainan	Wenchang	East Island's Forest Farm
XGB	14.6 %	75 %	79.5 %
ANN	12.8 %	77.5 %	79.6 %
RF	15.5 %	75.3 %	77 %

such cloud-free images are unavailable after major hazards.

Previous methods to recover cloud-covered information in remote sensing images rely on archived images of other periods that have no

land cover changes (Hu and Smith, 2018; Kang et al., 2016; Li et al., 2019). These methods cannot achieve fast forest-damage assessment in post-tropical cyclone, cloud contaminated optical images. Due to significant land cover changes caused by natural hazards, abundant pre-hazard images cannot be used to recover cloud-covered information in post-hazard images. To collect enough post-hazard images, longer time is needed making it impossible to rapidly map post-hazard forest damage holistically. The novelty of our work is to predict cloud-obscured forest damage with machine learning models by integrating remote sensing observations and related variables in cloud-free locations. The proposed machine learning-based method leverages influencing factors to construct models to estimate cloud-obscured damaged forests. This

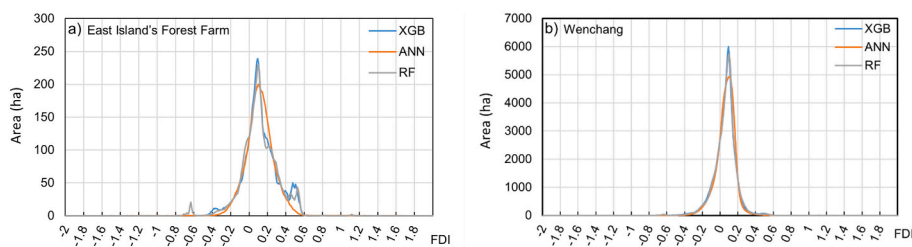


**Fig. 10.** Distribution of FDI predicted by XGB, ANN and RF in the East Island's Forest Farm (a). Distribution of FDI predicted by XGB, ANN and RF in Wenchang City (b). FDI counts the area in units of 0.01.

approach offers a feasible technical pathway for the rapid and efficient assessment of post-hazard vegetation damage.

### 5.2. Use of NDVI on mapping forest damage

This study utilises  $\Delta$ NDVI as a simple indicator for forest damage (FDI), which may be improved by using other biophysical parameters (e.g., above ground biomass). NDVI is a well-established index to monitor vegetation change with satellite images (Bartold, 2012; Bochenek et al., 2015a; Huang et al., 2021), whereby a significant NDVI decrease in forests during natural hazards are highly likely to be linked to forest damage owing to a near-total loss of leaves.

NDVI saturation in dense vegetation and soil reflectance in low vegetation cover may limit NDVI's sensitivity to forest damage (Liu and Huete, 1995). NDVI saturation could lead to an underestimation of forest damage in less-affected dense forests and soil reflectance could cause errors in low vegetation covered regions. Integrating other indices, such as the Enhanced Vegetation Index (EVI) or the Normalized Burn Ratio (NBR), or using a multi-sensor approach, may solve these problems to some extent (Escuin et al., 2008; Liu et al., 2017; Rogan et al., 2011). NDVI saturation and soil reflectance did not significantly affect the mapping of severe forest damage in this study, particularly where dense forests underwent extensive or near-complete destruction. These heavily impacted regions warrant greater stakeholder attention compared to areas exhibiting minimal damage or sparse vegetation. As this study aims to provide a workflow to overcome clouds in post-hazard damage assessment, employing these more effective indices (e.g., EVI and NBR) could warrant future research.

### 5.3. Considerations on machine learning and an $\Delta$ NDVI threshold

Model prediction uncertainty may stem from training dataset limitations. Relying on a single post-event image may introduce data bias, because sample points may not fully represent the full spectrum of vegetation characteristics from across the prediction area. This may be an inherent challenge in rapid post-event forest damage mapping depending on the location of cloud-free pixels. Using more advanced deep learning models (Qi et al., 2020) and optimizing the training set construction by considering the distribution of characteristic factors within the prediction area, a strategy successfully applied in landslide hazard prediction (Yang et al., 2023) may further enhance model performance. Additionally, uncertainties in meteorological data and the time lag between the acquisition of input factors (e.g. topography and canopy height) and the disaster event may lead to discrepancies between model predictions and actual conditions. To mitigate these uncertainties, the use of the most accurate and up-to-date data should always be a priority.

Threshold selection is another critical factor limiting the accuracy of disaster-affected area predictions. Despite a significant NDVI decrease indicating forest damage, the use of more subtle NDVI change may be complex. Defining a threshold to differentiate normal NDVI variations from confirmed disaster effects could be challenging. To address this, we attempted to infer a suitable forest damage threshold by combining manually collected statistics of affected areas. Although potentially suboptimal, this threshold was used to estimate potential forest damage across the island. Currently, there is not a universal threshold of  $\Delta$ NDVI to identify forest damage. Future work should focus on obtaining rapid and accurate ground-truth data from smaller, representative regions. This would enable back-calculation and refinement of  $\Delta$ NDVI thresholds to improve their applicability for larger-scale damage assessment.

### 5.4. Potential applications

Our work demonstrated a timely assessment of forest damage after a major tropical cyclone, though a strength of this method is that it can be applied to a broad range of natural hazards, such as earthquakes and

landslides. Major mountain earthquakes could trigger numerous co-seismic landslides damaging large area of forests, such as the 2008 Wenchuan earthquake-triggered landslides that damaged >1000 km<sup>2</sup> vegetation scattering over some 100,000 km<sup>2</sup> (Cui et al., 2012). Rapid and holistic mapping of these landslides was challenging and time-consuming given the complex topography and large spatial extent (Xu et al., 2014). Our proposed workflow could have benefitted this scenario by combining remote sensing and machine learning to fill the data gap caused by clouds or acquisitions. Another scenario would be to map wildfire-burned forests (Bhadoria et al., 2021), where heavy smoke may obscure satellite images and hinder the mapping of fire-damaged forests. Our workflow has the capacity to assimilate partial remote sensing observation with machine learning models to offer a more holistic understanding of fire-damaged forests. Future extension of our proposed scheme to internationally well-known services such as the PLOWET (Dabrowska-Zielinska et al., 2016) and the Copernicus Emergency Management Service (CEMS, <https://emergency.copernicus.eu/>) would benefit the public at large.

## 6. Conclusion

After the September 2024 Typhoon Yagi in Hainan, there is a great urgency to map damaged forests across the entire hazard-affected area with a limited number of cloud-contaminated, post-hazard remote sensing data. This study proposes a method to solve this problem. This method can rapidly and objectively assess pixels covered by clouds by interpolating observations from post-hazard, cloud-free pixels with three machine learning models (XGB, RF and ANN). Among these models, XGB and RF demonstrated superior predictive performances than ANN by demonstrating higher consistencies in estimating typhoon-affected forest areas. The analysis results indicate that the northeast part of the Hainan Island, particularly Wenchang City and the East Island's Forest Farm, suffered the most severe damage, with 75.0 %–75.3 % of the forest in Wenchang City negatively affected. This study found that the area of forest damage on Hainan Island with a damage index greater than 0 ranged from 3164.30 km<sup>2</sup> to 3361.38 km<sup>2</sup>, accounting for 14.6 % to 15.5 % of the island's total forest area.

Additionally, the study highlights that pre-hazard NDVI, and wind velocity are key factors in predicting forest damage. Notably, we also observed an increase in NDVI in some areas outside the typhoon's direct path, which may be related to the abundant rainfall and moderate wind disturbance brought by the typhoon, which warrants further investigation. Overall, this study provides a reliable framework for the rapid assessment of post-typhoon forest damage, overcoming the limitations posed by cloud cover in optical remote sensing imagery. It also offers valuable insights for efficient disaster response and forest management.

## Funding

This research was funded by the National Natural Science Foundation of China [No. 42407257] and the National Key Research and Development Program of China [No. 2024YFC3012603–04]

## CRediT authorship contribution statement

**Tianchu Wang:** Writing – review & editing, Writing – original draft, Visualization, Validation, Software, Methodology, Formal analysis, Data curation, Conceptualization. **Wentao Yang:** Writing – review & editing, Project administration, Methodology, Investigation, Funding acquisition, Conceptualization. **Ziteng Xu:** Validation, Software, Resources, Methodology, Data curation. **Wenwen Qi:** Software, Resources, Methodology, Funding acquisition, Conceptualization. **Liam Taylor:** Writing – review & editing, Validation. **Ming Wang:** Project administration, Investigation, Funding acquisition. **Wei Wu:** Project administration, Investigation, Funding acquisition.

## Declaration of competing interest

The authors declare that they have no known competing financial interests or personal relationships that could have appeared to influence the work reported in this paper.

## Data availability

The 30m Digital Elevation Model (DEM) data is sourced from the Shuttle Radar Topography Mission (SRTM) and can be accessed through Google Earth Engine ([https://lpdaac.usgs.gov/products/nasadem\\_hgtv001/](https://lpdaac.usgs.gov/products/nasadem_hgtv001/)). Additionally, the 10m optical remote sensing data from Sentinel-2 is also available on Google Earth Engine. Furthermore, the ETH Global Sentinel-2 10m Canopy Height data from 2020 can be retrieved from Google Earth Engine (<https://gee-community-catalog.org/projects/canopy/>). The wind velocity and precipitation data are published by the China Meteorological Administration (<https://data.cma.cn/site/article/id/42383.html>). All data can be freely accessed via this link <https://data.mendeley.com/datasets/xmwv4pztjm/1>. Our GEE code can be found at <https://code.earthengine.google.com/87fc325c613a621789cea7e26d3c280f>.

## References

- Achu, A.L., Thomas, J., Aju, C.D., Gopinath, G., Kumar, S., Reghunath, R., 2021. Machine-learning modelling of fire susceptibility in a forest-agriculture mosaic landscape of southern India. *Eco. Inform.* 64, 101348.
- Anees, S.A., Mehmood, K., Khan, W.R., Sajjad, M., Alahmadi, T.A., Alharbi, S.A., Luo, M., 2024. Integration of machine learning and remote sensing for above ground biomass estimation through Landsat-9 and field data in temperate forests of the Himalayan region. *Eco. Inform.* 82, 102732.
- Ansari, R.A., Esimaje, T., Ibrahim, O.M., Mulrooney, T., 2025. Analysis of Forest change detection induced by hurricane Helene using remote sensing data. *Forests* 16 (5), 788.
- Bartold, M., 2012. Monitoring of forest damage in Poland and Slovakia based on Terra-MODIS satellite images. *Geoinform.* Issues 4 (1), 23–31.
- Bartold, M., Kluczek, M., 2024. Estimating of chlorophyll fluorescence parameter Fv/Fm for plant stress detection at peatlands under Ramsar convention with Sentinel-2 satellite imagery. *Eco. Inform.* 81, 102603.
- Bhadoria, R.S., Pandey, M.K., Kundu, P., 2021. RVFR: random vector forest regression model for integrated & enhanced approach in forest fires predictions. *Eco. Inform.* 66, 101471.
- Bhatia, K., Baker, A., Yang, W., Vecchi, G., Knutson, T., Murakami, H., Whitlock, C., 2022. A potential explanation for the global increase in tropical cyclone rapid intensification. *Nat. Commun.* 13 (1), 6626.
- Bochenek, Z., Ziolkowski, D., Bartold, M., 2015a. Forest condition assessment through analyzing relations between meteorological parameters describing climate changes and vegetation indices derived from low-resolution satellite data. In: 2015 IEEE International Geoscience and Remote Sensing Symposium (IGARSS). IEEE, pp. 3341–3344.
- Bochenek, Z., Ziolkowski, D., Bartold, M., 2015b. Application of NOAA AVHRR satellite images for studying various environmental and climatic conditions in polish forests. *Geoinform. Issues* 7 (1), 29–37.
- Breiman, L., 2001. Random forests. *Mach. Learn.* 45 (1), 5–32. <https://doi.org/10.1023/A:1010933404324>.
- Burrows, K., Marc, O., Andermann, C., 2023. Retrieval of monsoon landslide timings with Sentinel-1 reveals the effects of earthquakes and extreme rainfall. *Geophys. Res. Lett.* 50 (16), e2023GL104720. <https://doi.org/10.1029/2023GL104720>.
- Chen, T., Guestrin, C., 2016. XGBoost: A scalable tree boosting system. In: Proceedings of the 22nd ACM SIGKDD International Conference on Knowledge Discovery and Data Mining, pp. 785–794. <https://doi.org/10.1145/2939672.2939785>.
- Chen, X., Avtar, R., Umarhadi, D.A., Louw, A.S., Shrivastava, S., Yunus, A.P., Khedher, K. M., Takemi, T., Shibata, H., 2022. Post-typhoon forest damage estimation using multiple vegetation indices and machine learning models. *Weather Clim. Extremes* 38, 100494. <https://doi.org/10.1016/j.wace.2022.100494>.
- China Meteorological Administration, 2024. Meteorological Data Service Bulletin: Impact Report on Typhoon "Yagi" Before Landfall. <https://data.cma.cn/site/article/id/42381.html>.
- China Meteorological News Press, 2024. Facing the Strongest Autumn Typhoon "Yagi" Landing in China: Meteorological Departments Make Every Effort to Prevent the Impact of Typhoon Wind and Rain. [https://www.cma.gov.cn/ztbd/2024zt/20240430/202409/t20240918\\_6589746.html](https://www.cma.gov.cn/ztbd/2024zt/20240430/2024043002/202409/t20240918_6589746.html).
- Cui, P., Lin, Y.M., Chen, C., 2012. Destruction of vegetation due to geo-hazards and its environmental impacts in the Wenchuan earthquake areas. *Ecol. Eng.* 44, 61–69.
- Dabrowska-Zielinska, K., Bartold, M., Gurdak, R., 2016. POLWET—system for new space-based products for wetlands under RAMSAR convention. *Geoinf. Issues* 8, 25–35.
- Dimson, M., Cavanaugh, K.C., von Allmen, E., Burney, D.A., Kawelo, K., Beachy, J., Gillespie, T.W., 2024. Monitoring native, non-native, and restored tropical dry forest with Landsat: a case study from the Hawaiian islands. *Eco. Inform.* 83, 102821.
- Escuin, S., Navarro, R., Fernández, P., 2008. Fire severity assessment by using NBR (normalized burn ratio) and NDVI (normalized difference vegetation index) derived from LANDSAT TM/ETM images. *Int. J. Remote Sens.* 29 (4), 1053–1073.
- Eskandari, S., Sarab, S.A.M., 2022. Mapping land cover and forest density in Zagros forests of Khuzestan province in Iran: a study based on Sentinel-2, Google earth and field data. *Eco. Inform.* 70, 101727.
- Feng, Y., Negrón-Juárez, R.L., Chambers, J.Q., 2020. Remote sensing and statistical analysis of the effects of hurricane María on the forests of Puerto Rico. *Remote Sens. Environ.* 247, 111940. <https://doi.org/10.1016/j.rse.2020.111940>.
- Guo, P., Zhao, X., Shi, J., Huang, J., Tang, J., Zhang, R., Zeng, J., 2021. The influence of temperature and precipitation on the vegetation dynamics of the tropical island of Hainan. *Theor. Appl. Climatol.* 143, 429–445.
- Hainan Historical and Cultural Website, 2024. Overview of Hainan. <https://www.hainan.gov.cn/hainan/hngl/201809/02b6b908146c4ce89c0dbd1fad7720a6.shtml?ddt=ab=true>.
- Hainan Provincial Forestry Bureau, 2023. 2023 Hainan Forestry and Grass Yearbook. [https://lyj.hainan.gov.cn/xxgk/tjxx/202405/t20240515\\_3663519.html](https://lyj.hainan.gov.cn/xxgk/tjxx/202405/t20240515_3663519.html).
- Hayashi, M., Saigusa, N., Oguma, H., Yamagata, Y., Takao, G., 2015. Quantitative assessment of the impact of typhoon disturbance on a Japanese forest using satellite laser altimetry. *Remote Sens. Environ.* 156, 216–225. <https://doi.org/10.1016/j.rse.2014.09.028>.
- Hou, Q., Ji, Z., Yang, H., Yu, X., 2022. Impacts of climate change and human activities on different degraded grassland based on NDVI. *Sci. Rep.* 12 (1), 15918. <https://doi.org/10.1038/s41598-022-19943-6>.
- Howe, J., Merchant, S., Hernández, W.J., Pessutti, J., Groffman, P., 2025. Assessing mangrove canopy height and health changes in Puerto Rico post-hurricane Maria using remote-sensing techniques. *Ecosphere* 16 (3), e70226.
- Hu, T., Smith, R.B., 2018. The impact of hurricane Maria on the vegetation of Dominica and Puerto Rico using multispectral remote sensing. *Remote Sensing* 10 (6), 6. <https://doi.org/10.3390/rs10060827>.
- Huang, S., Tang, L., Hupy, J.P., Wang, Y., Shao, G., 2021. A commentary review on the use of normalized difference vegetation index (NDVI) in the era of popular remote sensing. *J. For. Res.* 32 (1), 1–6. <https://doi.org/10.1007/s11676-020-01155-1>.
- Kang, Y., Pan, L., Chen, Q., Zhang, T., Zhang, S., Liu, Z., 2016. Automatic mosaicking of satellite imagery considering the clouds. In: ISPRS Annals of the Photogrammetry, Remote Sensing and Spatial Information Sciences, III–3. XXIII ISPRS Congress, Commission III (Volume III-3) - 12&ndash;19 July 2016, Prague, Czech Republic, pp. 415–421. <https://doi.org/10.5194/isprs-annals-iii-3-415-2016>.
- Khajwal, A.B., Noshadravan, A., 2021. An uncertainty-aware framework for reliable disaster damage assessment via crowdsourcing. *Int. J. Disaster Risk Reduc.* 55, 102110.
- Konatowska, M., Młynarczyk, A., Kowalewski, W., Rutkowski, P., 2023. NDVI as a potential tool for forecasting changes in geographical range of sycamore (*Acer pseudoplatanus* L.). *Sci. Rep.* 13 (1), 19818. <https://doi.org/10.1038/s41598-023-46301-x>.
- Lang, N., Jetz, W., Schindler, K., Wegner, J.D., 2023. A high-resolution canopy height model of the earth. *Nature Ecol. Evol.* 7 (11), 1778–1789. <https://doi.org/10.1038/s41559-023-02206-6>.
- Lee, M.-F., Lin, T.-C., Vadeboncoeur, M.A., Hwong, J.-L., 2008. Remote sensing assessment of forest damage in relation to the 1996 strong typhoon herb at Lienhuachi experimental Forest, Taiwan. *Forest Ecol. Manage.* 255 (8–9), 3297–3306. <https://doi.org/10.1016/j.foreco.2008.02.010>.
- Leisenheimer, L., Wellmann, T., Jänicke, C., Haase, D., 2024. Monitoring drought impacts on street trees using remote sensing-disentangling temporal and species-specific response patterns with Sentinel-2 imagery. *Eco. Inform.* 82, 102659.
- Li, J., Wu, Z., Hu, Z., Zhang, J., Li, M., Mo, L., Molinier, M., 2020. Thin cloud removal in optical remote sensing images based on generative adversarial networks and physical model of cloud distortion. *ISPRS J. Photogramm. Remote Sens.* 166, 373–389. <https://doi.org/10.1016/j.isprsjprs.2020.06.021>.
- Li, X., Feng, R., Guan, X., Shen, H., Zhang, L., 2019. Remote sensing image mosaicking: achievements and challenges. *IEEE Geosci. Remote Sens. Magazine* 7 (4), 8–22. <https://doi.org/10.1109/MGRS.2019.2921780>.
- Li, X., Xu, J., Jia, Y., Liu, S., Jiang, Y., Yuan, Z., Ye, Y., 2024. Spatio-temporal dynamics of vegetation over cloudy areas in Southwest China retrieved from four NDVI products. *Eco. Inform.* 81, 102630.
- Liu, H.Q., Huete, A., 1995. A feedback based modification of the NDVI to minimize canopy background and atmospheric noise. *IEEE Trans. Geosci. Remote Sens.* 33 (2), 457–465.
- Liu, X., Jiang, W., Li, J., Wang, W., 2017. Evaluation of the vegetation coverage resilience in areas damaged by the Wenchuan earthquake based on MODIS-EVI data. *Sensors* 17 (2), 259.
- Liu, Z., Xu, L., Lu, Q., 2024. Comprehensive typhoon hazard zoning in China based on historical records. *Geomat. Nat. Haz. Risk* 15 (1), 2300813. <https://doi.org/10.1080/19475705.2023.2300813>.
- Louis, J., Devignot, O., Pessiot, L., 2021. Level-2a Algorithm Theoretical Basis Document. Santa Rosa, CA, USA, Remote Sensing Systems, p. 78.
- Lu, L., Wu, C., Di, L., 2020. Exploring the spatial characteristics of typhoon-induced vegetation damage in the southeast coastal area of China from 2000 to 2018. *Remote Sens. (Basel)* 12 (10), 10. <https://doi.org/10.3390/rs12101692>.
- Main-Knoorn, M., Pflug, B., Louis, J., Debaecker, V., Müller-Wilm, U., Gascon, F., 2017. Sen2Cor for sentinel-2. In: Image and Signal Processing for Remote Sensing XXIII, 10427. SPIE, pp. 37–48.

- Mehmood, K., Anees, S.A., Muhammad, S., Hussain, K., Shahzad, F., Liu, Q., Ansari, M.J., Alharbi, S.A., Khan, W.R., 2024. Analyzing vegetation health dynamics across seasons and regions through NDVI and climatic variables. *Sci. Rep.* 14 (1), 11775. <https://doi.org/10.1038/s41598-024-62464-7>.
- Mendelsohn, R., Emanuel, K., Chonabayashi, S., Bakkensen, L., 2012. The impact of climate change on global tropical cyclone damage. *Nat. Clim. Chang.* 2 (3), 205–209.
- Meraner, A., Ebel, P., Zhu, X.X., Schmitt, M., 2020. Cloud removal in Sentinel-2 imagery using a deep residual neural network and SAR-optical data fusion. *ISPRS J. Photogram. Rem. Sens.* 166, 333–346. <https://doi.org/10.1016/j.isprsjprs.2020.05.013>.
- Qi, W., Xu, C., 2020. Automatic recognition method for fire passing range and burning degree of forest fire [CN112613347B]. *National Inst. Nat. Hazards.* (2021-07-27).
- Qi, W., Wei, M., Yang, W., Xu, C., Ma, C., 2020. Automatic mapping of landslides by the ResU-net. *Remote Sens. (Basel)* 12 (15), 15. <https://doi.org/10.3390/rs12152487>.
- Rogan, J., Schneider, L., Christman, Z., Millones, M., Lawrence, D., Schmook, B., 2011. Hurricane disturbance mapping using MODIS EVI data in the southeastern Yucatán, Mexico. *Remote Sens. Lett.* 2 (3), 259–267.
- Salim, M.Z., Al Kafy, A., Altuwajri, H.A., Miah, M.T., Jodder, P.K., Rahaman, Z.A., 2024. Quantitative assessment of hurricane Ian's damage on urban vegetation dynamics utilizing Landsat 9 in Fort Myers, Florida. *Phys. Chem. Earth, Parts A/B/C* 136, 103750.
- Sarkar, M.S., Majhi, B.K., Pathak, B., Biswas, T., Mahapatra, S., Kumar, D., Nautiyal, S., 2024. Ensembling machine learning models to identify forest fire-susceptible zones in Northeast India. *Eco. Inform.* 81, 102598.
- Schnur, M.T., Xie, H., Wang, X., 2010. Estimating root zone soil moisture at distant sites using MODIS NDVI and EVI in a semi-arid region of southwestern USA. *Eco. Inform.* 5 (5), 400–409.
- Setiono, R., Leow, W.K., Zurada, J.M., 2002. Extraction of rules from artificial neural networks for nonlinear regression. *IEEE Trans. Neural Networks* 13 (3), 564–577. <https://doi.org/10.1109/TNN.2002.1000125>.
- Sobel, A.H., Camargo, S.J., Hall, T.M., Lee, C.Y., Tippet, M.K., Wing, A.A., 2016. Human influence on tropical cyclone intensity. *Science* 353 (6296), 242–246.
- Sonet, M.S., Hasan, M.Y., Chakma, S., Al Kafy, A., 2024. Assessing tropical cyclone impacts in coastal Bangladesh: a change detection analysis on cyclone bulbul using geospatial analysis and remote sensing techniques. *Int. J. Disaster Risk Reduc.* 112, 104726.
- Sun, Z., Chang, N.B., Opp, C., Hennig, T., 2011. Evaluation of ecological restoration through vegetation patterns in the lower Tarim River, China with MODIS NDVI data. *Eco. Inform.* 6 (2), 156–163.
- Tanase, M.A., Aponte, C., Mermoz, S., Bouvet, A., Le Toan, T., Heurich, M., 2018. Detection of windthrows and insect outbreaks by L-band SAR: a case study in the Bavarian Forest National Park. *Remote Sens. Environ.* 209, 700–711. <https://doi.org/10.1016/j.rse.2018.03.009>.
- Tomppo, E., Ronoud, G., Antropov, O., Hytönen, H., Praks, J., 2021. Detection of Forest windstorm damage with multitemporal SAR data—a case study: Finland. *Remote Sens. (Basel)* 13 (3), 3. <https://doi.org/10.3390/rs13030383>.
- Upadhyay, V., Kumar, A., 2018. Hyperspectral remote sensing of forests: technological advancements, Opportunities and challenges. *Earth Sci. Inform.* 11 (4), 487–524. <https://doi.org/10.1007/s12145-018-0345-7>.
- Wang, M., Xu, H., 2018. Remote sensing-based assessment of vegetation damage by a strong typhoon (Meranti) in Xiamen Island, China. *Natural Hazards* 93 (3), 1231–1249. <https://doi.org/10.1007/s11069-018-3351-7>.
- Xu, C., Xu, X., Yao, X., Dai, F., 2014. Three (nearly) complete inventories of landslides triggered by the may 12, 2008 Wenchuan mw 7.9 earthquake of China and their spatial distribution statistical analysis. *Landslides* 11, 441–461.
- Xu, G.X., Guo, Q.S., Niu, S.K., Pei, S.X., Zhu, L., Zhu, N.N., 2013. Research on climate change characteristics of different climatic regions in Hainan Island in the last 50 years. *J. Nat. Resour.* 28 (5), 799–810.
- Xu, X., Sun, D., Guo, T., 2015. A systemic analysis of typhoon risk across China. *Nat. Hazards* 77 (1), 461–477. <https://doi.org/10.1007/s11069-015-1586-0>.
- Yang, H., Shi, P., Quincey, D., Qi, W., Yang, W., 2023. A heterogeneous sampling strategy to model earthquake-triggered landslides. *Int. J. Disaster Risk Sci.* 14 (4), 636–648. <https://doi.org/10.1007/s13753-023-00489-8>.
- Yang, J., Huang, X., 2021. The 30&thinspm; annual land cover dataset and its dynamics in China from 1990 to 2019. *Earth Syst. Sci. Data* 13 (8), 3907–3925. <https://doi.org/10.5194/essd-13-3907-2021>.
- Yang, W., Wang, M., Shi, P., 2013. Using MODIS NDVI time series to identify geographic patterns of landslides in vegetated regions. *IEEE Geosci. Remote Sens. Lett.* 10 (4), 707–710. <https://doi.org/10.1109/LGRS.2012.2219576>.
- Yang, X., Chen, Z., Li, D., 2021. Classification and distribution of vegetation in Hainan, China. *Scientia Sinica Vitae* 51 (3), 321–333. <https://doi.org/10.1360/SSV-2020-0286>.
- Zahura, F.T., Bisht, G., Li, Z., McKnight, S., Chen, X., 2024. Impact of topography and climate on post-fire vegetation recovery across different burn severity and land cover types through random forest. *Eco. Inform.* 82, 102757.
- Zhang, K., Zhu, C., Li, J., Shi, K., Zhang, X., 2024. Reconstruction of dense time series high spatial resolution NDVI data using a spatiotemporal optimal weighted combination estimation model based on Sentinel-2 and MODIS. *Eco. Inform.* 82, 102725.
- Zhang, X., Chen, G., Cai, L., Jiao, H., Hua, J., Luo, X., Wei, X., 2021. Impact assessments of typhoon Lekima on Forest damage in subtropical China using machine learning methods and Landsat 8 OLI imagery. *Sustainability* 13 (9), 9. <https://doi.org/10.3390/su13094893>.
- Zhang, X., Jiao, H., Chen, G., Shen, J., Huang, Z., Luo, H., 2022. Forest damage by super typhoon Rammasun and post-disturbance recovery using Landsat imagery and the machine-learning method. *Remote Sens. (Basel)* 14 (15), 15. <https://doi.org/10.3390/rs14153826>.
- Zhu, Z., Woodcock, C.E., 2014. Continuous change detection and classification of land cover using all available Landsat data. *Remote Sens. Environ.* 144, 152–171.